

The Dynamics of the Transverse Optical Flux in Random Media

Y. Ke¹, N. Bhattacharya¹, and F. Maucher^{1*}

¹*Faculty of Mechanical Engineering; Department of Precision and Microsystems Engineering, Delft University of Technology, 2628 CD, Delft, The Netherlands*

We study the evolution of the kinetic energy (or gradient norm) of an incident linearly polarised monochromatic wave propagating in correlated random media. We explore the optical flux transverse to the mean Poynting flux at the paraxial-nonparaxial (vectorial) transition along with vortex counting and identify universal features in the dynamics. The vortex number appears to increase with a cubic root for sufficiently small correlation length. Furthermore, a kink appears in nucleation rate at the position of maximum scintillation upon increasing correlation length. A driven steady state is reached due to the filtering of evanescent waves upon propagation. Finally, we present the spectrum of the incompressible kinetic energy and how it evolves from the paraxial case to that of a random field.

The propagation of light in a medium causes microscopic superposition between the incident field and the atomic or molecular dipole fields [1]. Optical media are usually dense; i.e. the interparticle separation is usually much smaller than the wavelength, thus each particle sees the secondary fields of a large neighborhood of particles. This gives rise to an overall macroscopic response in the form of a refractive index of the medium. Heterogeneity of the media leads to modulations of the refractive index [2], which to lowest order can be described as correlated random perturbations. The propagation of light in random media is complex, as it often involves taking into account multiple scattering and material properties [1, 3–5]. The effects on the propagation of light in random media became further accessible due to the availability of coherent monochromatic sources. Intriguing phenomena emerge such as atmospheric scintillation [6], branching of light [7, 8] or Anderson localisation [9–12]. Through multichannel interference [13] light propagation in random medium can act focusing like a lens [14, 15]. Furthermore, spectrometers can be based on random media [16, 17]. Upon traveling through random media, vortices [18] nucleate in light. Optical vortices are quantized, point-like null regions of intensity surrounded by azimuthal phase ramp, and thus determine the azimuthal flow of light. Vortices can be thought of as a singular skeleton [19] for the speckle pattern, carrying information that is complementary to the amplitude, employed for e.g. multiplexing [20]. Vortices permit advanced trapping control [21], and the associated momentum can even be entangled on the single photon level [22]. Quantized vortices also occur in ultra-cold quantum fluids [23], where instead of propagating through a random medium they can be nucleated via optical stirring [24] or magnetic quenching leading to quantum turbulence [25]. Vortex statistics of optical beams after a planar speckle field have been extensively studied [26, 27]. The interplay between optical speckle and vortices has been explored in volumetric random fields [28, 29] and the ensemble dynamics of point-vortices in speckle fields studied [30].

In this work, we aim at further understanding and sta-

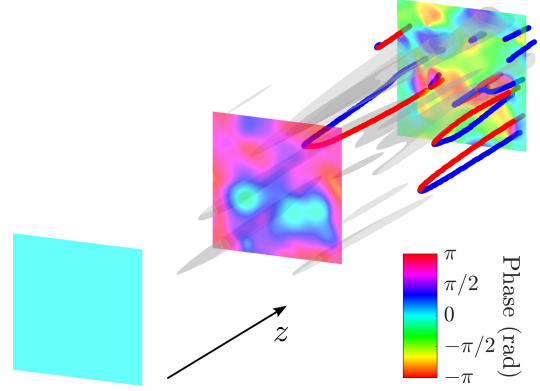


FIG. 1. Propagation of an initially linearly polarized plane wave in a random medium. The planes depict the phase, the lines correspond to vortex lines [red (blue) topological charge 1 (−1)] and the grey iso-surface depicts the intensity, showing speckle formation.

tistically characterizing the phase of light as it evolves upon the propagation of monochromatic waves in random media, as visualised in Fig. 1. We consider randomness to be fully determined by amplitude and correlation length of the refractive index [2]. We approach this problem by considering "kinetic energy", i.e. the gradient norm of the electric field, as it contains both amplitude- and phase-information, in addition to vortex counting upon propagation. For the early propagation, we compare numerics with a paraxial analytical expression for the kinetic energy. We then characterise the dynamics by the number of vortices as function of propagation distance in the medium. Finally, we consider the energy spectrum - i.e. incompressible kinetic energy as function of the wave vector - borrowing methods from quantum turbulence theory [31].

From Maxwell's equations it is simple to find that the wave propagation of the electrical field $\mathbf{E}(\mathbf{r})$ in a linear, non-magnetizable medium is governed by the following vector wave equation:

$$\nabla \times \nabla \times \mathbf{E}(\mathbf{r}) - k(\mathbf{r})^2 \mathbf{E}(\mathbf{r}) = 0. \quad (1)$$

Here, $\mathbf{r} = (x, y, z)$, $\mathbf{k}(\mathbf{r})$ is the wave vector with modulus $k(\mathbf{r}) = 2\pi n(\mathbf{r})/\lambda$ where λ is the wavelength. The refractive index is given by $n(\mathbf{r}) = n_0 + \eta(\mathbf{r})$ [32], where n_0 is the constant background refractive index and $\eta(\mathbf{r})$ the spatially-dependent deviation. We assume that the direction of the mean Poynting flux is equivalent to the z -direction. We assume $\eta(\mathbf{r})$ to be Gaussian correlated, i.e.

$$\langle \eta(\mathbf{r})\eta(\mathbf{r}') \rangle = C(\mathbf{r} - \mathbf{r}'); C(\mathbf{r}) = \frac{\kappa^2 e^{-\frac{r^2}{2\sigma^2}}}{(2\pi\sigma^2)^{3/2}} \quad (2)$$

Here, $\langle \cdot \rangle$ denotes the ensemble average, and κ is the coupling strength characterising the amplitude of the noise. Hence, Eq. (1) has two free parameters σ/λ and $\kappa/\lambda^{3/2}$.

To propagate the wave in the random medium, we use the modified Born series approach described in [33, 34]. We assume the source to be a linearly polarised plane wave with polarisation along the x -axis. We typically use 64 cores for simulating a grid of $N_x = N_y = 256 - 512$ and $N_z = 512 - 4096$ points and roughly 100 - 40000 iterations. Without loss of generality, the background refractive index of all media is set to $n_0 = 1.5$. We use periodic boundary conditions in the $\mathbf{r}_\perp = (x, y)$ -plane transverse to the mean Poynting flux to mimic the thermodynamic limit - i.e. an infinite transverse plane \mathcal{A} - and absorbing boundary condition in the z direction parallel to the mean Poynting flux.

We use this framework to investigate the propagation. For convenience, we restrict our consideration to the original x -polarisation and define the transverse kinetic energy per unit area as

$$E_{\text{kin}}(z) = \lim_{\mathcal{A} \rightarrow \infty} \frac{1}{\mathcal{A}} \int_{\mathcal{A}} |\nabla_\perp E_x(\mathbf{r}_\perp, z)|^2 d^2 r_\perp. \quad (3)$$

Within paraxial approximation and linearisation in η , employing the Furutsu-Novikov-Donsker formula [35, 36], akin to [37] we can find an approximation for the slope of the kinetic energy per unit area in the z direction as follows:

$$\partial_z \langle E_{\text{kin}} \rangle = -\frac{4\sqrt{2}\pi^{5/2}\sigma\mathcal{I}_x}{\lambda^2} \nabla_\perp^2 C \Big|_{\mathbf{r}=0} = \frac{4\pi\kappa^2}{\sigma^4\lambda^2} \mathcal{I}_x. \quad (4)$$

Here, we introduced the intensity \mathcal{I}_i or average power per area \mathcal{A} as $\mathcal{I}_i = \lim_{\mathcal{A} \rightarrow \infty} \frac{1}{\mathcal{A}} \int_{\mathcal{A}} |E_i|^2 d^2 r_\perp$. The detailed derivation for Eq. (4) is shown in the supplement [38].

The comparison between the analytical prediction and numerics is shown in Fig. 2(a,b), where the quantity $\mathcal{I}^0 = \mathcal{I}(\eta = 0)$ was introduced for normalisation purposes. From the paraxial consideration Eq. (4), one would expect a scaling $\sim \kappa^2 \mathcal{I}_x / \sigma^4 \lambda^2$ of the slope. Yet, evidently, this scaling is violated quickly once the propagation becomes nonparaxial and vectorial, leading to a significant mismatch. To illustrate that we colored the

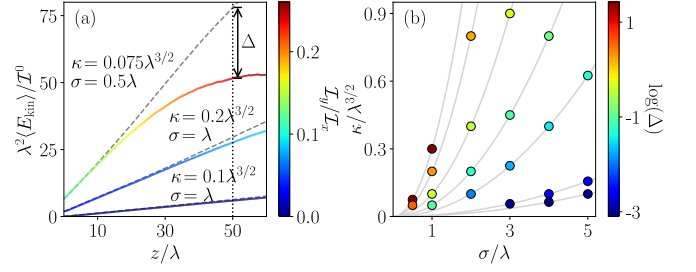


FIG. 2. (a) Comparison of numerical simulations (solid lines) and analytical predictions (dashed lines) for the evolution of the ensemble-averaged kinetic energy at the initial stage. Δ denotes the difference evaluated at $z = 50\lambda$. (b) The values of Δ for various σ and κ , represented on a logarithmic scale. The grey lines represent iso-lines where $\kappa^2\lambda/\sigma^4$ is constant. The ensemble average was performed over 10 realizations.

numerical data with $\mathcal{I}_y/\mathcal{I}_x$. The difference Δ evaluated as function of κ and σ is illustrated by the colormap in Fig. 2(b) in logarithmic scale. We see that decreasing σ or increasing κ results in the increase of the difference Δ . This can be expected, as both lead to a deviation from paraxiality. To further qualitatively interpret the result, consider the grey lines representing isolines, where the slope is predicted to be equal. We observe, that the difference Δ is roughly equal on these lines.

Subsequently, the increase in kinetic energy leads to the nucleation of vortex pairs. We would like to proceed now with characterising the dynamics using the number of vortices N_v . Fig. 3(a) depicts the vortex density per unit area, $\rho_v = \lim_{\mathcal{A} \rightarrow \infty} N_v(\mathcal{A})/\mathcal{A}$ as function of the propagation distance z . For that matter, we chose a set of realisations with fixed autocorrelation $C(0)$. We see that three stages of the dynamics become apparent. In the initial stage, where the paraxial approximation still holds, only a few vortices start to nucleate due to the accumulation of kinetic energy (cf. Fig. 2).

After that, there is an intermediate region, which features a more rapid increase in vortex number upon propagation. In case of sufficiently small correlation length ($\sigma = 0.5\lambda$, orange line), we find that this increase is approximately a radical function, with $\rho_v \lambda^2 \propto (z/\lambda - z_{\text{cr}}/\lambda)^\beta$ and critical exponent $\beta \approx 1/3$. Similar values for β can be found for other κ , provided in the supplement [38]. The dynamics mimics critical behaviour in the Ising model [39, 40], where the order-parameter vortex density can be associated with magnetisation and propagation distance with temperature. The increase in vortex number appears to be inhibited for a short propagation interval if the correlation length is sufficiently large. The position where this thwarting occurs coincides with the point of maximum scintillation. The latter is shown in Fig. 3(c), where the scintillation index [6] is defined as $S_x(z) = \frac{\langle \mathcal{I}_x(z)^2 \rangle}{\langle \mathcal{I}_x(z) \rangle^2} - 1$. This peak has been identified as a universal feature when studying propagation in random

media in a classical context [41], around which a delay in the creation of branches has been observed. This same universality appears in the number of vortices generated upon propagation as well.

Upon further propagation, it appears that although the random refractive index continues to drive the nucleation of more vortices, the dynamics leads to a new equilibrium, a driven steady-state where the nucleation and reconnection rate become equal. Thereby, we find a plateau of a roughly constant number of vortices upon propagation in Fig. 3(a). That is due to that the spatial spectrum of the wave can only broaden upon propagation until the evanescent limit is reached, and a further increase in complexity of the propagating wave function per unit area is not possible.

To estimate the asymptotic limit of the number of vortices per unit area, we first generate a well-resolved complex random field with Gaussian distributed random amplitude and uniformly distributed random phase in the range $[-\pi, \pi)$. Then, we apply a spectral filter $\sqrt{k_x^2 + k_y^2} < \frac{2\pi n^*}{\lambda}$ to the wave in the Fourier domain to remove parts of the wave that are beyond the evanescent limit. It is not *a priori* clear what we ought to use for n^* . Employing $n^* = n_0$ leads to a cut-off radius that is spectrally too narrow, and thus we expect that using this cut-off will amount to a lower estimate for the predicted number of vortices per unit area. This is indeed what we observe in Fig. 3(a) (dash-dotted line). Alternatively, considering a spectrally broader interval by using $n^* = n_0 + \sqrt{C(0)}$, leads to the (dashed line) and, unlike the first prediction, contains information about the correlation length and coupling strength. Both of these estimates neglect "outliers" in spatial Fourier space, and thus both seem to underestimate the number of vortices. However, by choosing random numbers that are equally likely in the whole spectral disk in Fourier space we slightly overestimate the complexity of the wave. These two estimates provide an interval within which the results of rigorous numerical computation can be expected to lie as can be seen in Fig. 3(a).

Fig. 3(b) depicts how the asymptotic number of vortices per unit area depends on the coupling strength κ and correlation length σ more systematically. We notice that an increase in coupling strength for a fixed correlation length, as well as a decrease in correlation length whilst keeping the autocorrelation $\kappa/\sigma^{3/2}$ fixed, consistently leads to an increase in the number of vortices. Both of these trends are not captured fully in the approximate model, as $n^* = n_0$ does not capture any dependency on κ and σ . The approximation $n^* = n_0 + \sqrt{C(0)}$ predicts that there should be no change for fixed autocorrelation $\kappa/\sigma^{3/2}$ (horizontal line). Fig. 3(d) provides further context as to how vectorial the light becomes through scattering by displaying the ratio of the intensities $\mathcal{I}_y/\mathcal{I}_x$.

Finally, we would like to characterise the kinetic en-

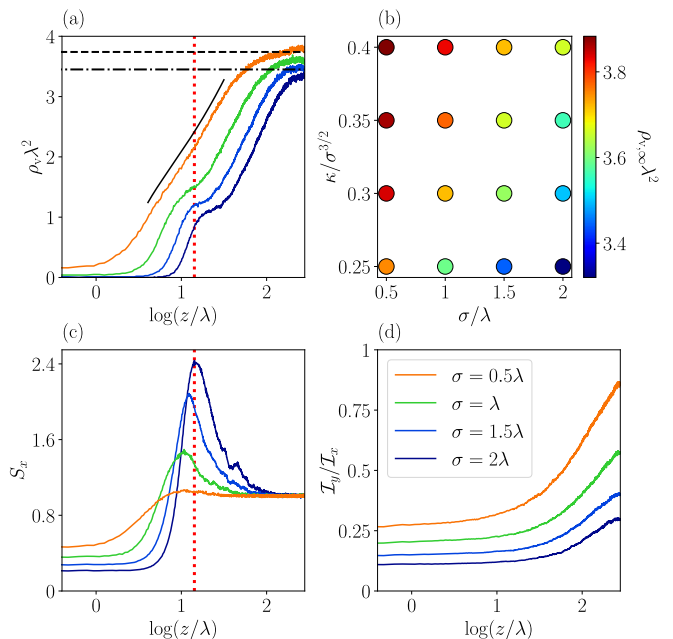


FIG. 3. (a) Evolution of vortex number per unit area ρ_v for $\sigma = 0.5\lambda, \lambda, 1.5\lambda, 2\lambda$ and $\kappa = 0.25\sigma^{3/2}$, where the black solid line shows the trend for 0.5λ . The dashed and dash-dotted horizontal lines are the estimations of $\rho_{v,\infty}$ obtained by applying two different filters to a random field in spatial Fourier domain. See (d) for the colors. (b) Values of the vortex density $\rho_{v,\infty}$ for various parameter sets of random media. (c) Shows the evolution of the scintillation index, the maximum of which (e.g. vertical dotted line for $\sigma = 2\lambda$) coinciding with the first branching point and the position of inhibited vortex nucleation. (d) shows the ratio of intensities in y and x polarisations for the four curves in (a).

ergy further and study its internal distribution in terms of the inverse length scale or the spatial Fourier wave vector. Similar to quantum turbulence theory [31] a more detailed characterisation can be achieved by studying the energy spectrum. The total kinetic energy of a field $E = Ae^{i\Phi}$ can be decomposed as $\int |\nabla_{\perp} E|^2 d^2 r_{\perp} = \int |\nabla_{\perp} A|^2 + |A \nabla_{\perp} \Phi|^2 d^2 r_{\perp}$. $\nabla_{\perp} \Phi$ represents the "velocity" of the flux in the transverse plane. Its value increases near the phase singularity. The amplitude-weighted velocity field $\mathbf{u} = A \nabla_{\perp} \Phi$ can be further decomposed into a compressible and an incompressible part using Helmholtz decomposition, $\mathbf{u} = \mathbf{u}^c + \mathbf{u}^i$. This can be expressed in components as $u_i = \partial_i f + \epsilon_{ij} \partial_j g = u_i^c + u_i^i$, where f, g are scalar functions. By construction, there is an incompressible \mathbf{u}^i or divergence-free part of the field \mathbf{u} that satisfies $\partial_i u_i^i = 0$, as well as a compressible or curl-free part \mathbf{u}^c satisfying $\epsilon_{ij} \partial_i u_j^c = 0$.

The kinetic energy of the incompressible part is defined as $E_{\text{kin}}^i = \int |\mathbf{u}^i(\mathbf{r}_{\perp})|^2 d^2 r_{\perp}$. It is useful to find its dependence on the modulus of the wavenumber k by integrating the incompressible field in Fourier domain over

the azimuthal angle in polar coordinates

$$E_{\text{kin}}^i(k) = k \int_0^{2\pi} |\hat{\mathbf{u}}^i(\mathbf{k})|^2 d\phi_k, \quad (5)$$

where $\hat{\mathbf{u}}^i(\mathbf{k}) = \mathcal{F}_{2d}\{\mathbf{u}^i(\mathbf{r}_\perp)\}$ is the two-dimensional Fourier transform of the incompressible field. In case of sufficiently large σ and sufficiently small κ when the wave propagation becomes effectively paraxial, the tail of the incompressible kinetic energy can be expected to mimic that of a single vortex. To match the two, we consider a finite single vortex with a Gaussian profile and the amplitude being a free parameter. Hence, we assume a quasi-linearly polarised beam with profile $E_x = r_\perp e^{-\frac{r_\perp^2}{\sigma^2}} e^{\pm i\theta}$ with $\theta = \arctan(y/x)$. In that case it is simple to find the incompressible kinetic energy as

$$E_{\text{kin}}^i(k) \propto \sigma^6 k^3 e^{-\frac{\sigma^2 k^2}{4}} \left[I_0\left(\frac{\sigma^2 k^2}{8}\right) - I_1\left(\frac{\sigma^2 k^2}{8}\right) \right]^2,$$

where I_j is the modified Bessel function of the first kind of order j . Thus, we chose the correlation length σ as the width of the Gaussian envelope. This expression asymptotically scales as $\sim k^{-3}$, and the peak is inversely proportional to length scale σ .

The comparison between theory and rigorous numerics of the incompressible kinetic energy spectrum for the paraxial case is shown in Fig. 4(a) for the case $\sigma = 5\lambda$ and $\kappa = 0.01\sigma^{3/2}$. To obtain this spectrum, we propagated an initially linearly polarised plane wave to $z = 310\lambda$. To compare numerics to theory, we multiplied the theoretical incompressible kinetic energy with a constant to match the peak value of the numerical one. We find that, indeed, the tail as well as the peak position k_{peak} is well-predicted by the analytical model of the single vortex. The peak corresponds to the inverse length scale at which energy is injected, i.e. proportional to $1/\sigma$. In fact, the analytical prediction yields $k_{\text{peak}} = 2\pi/\sqrt{8}\sigma$, shown as the dashed grey vertical line in Fig. 4(a).

Let us now consider the situation where the wave is nonparaxial and vectorial, shown in Fig. 4(a) at a propagation distance where the driven steady-state has been reached and with $\sigma = \lambda$ and $\kappa = 0.4\sigma^{3/2}$. It is numerically challenging to show the ultraviolet range up to the point where the asymptotic behavior k^{-3} becomes obvious. For achieving that, we used 128 cores and a grid of 1024^3 points and benchmarked against $512^2 \times 2048$. We would like to understand the numerical result (solid blue line) employing a suitable model (dashed blue line). We use again the method employed before to obtain a prediction for the number of vortices per unit area by considering a random field and spectrally filtering out the evanescent part. Note, that in this case the peak becomes completely independent of σ , and the only relevant length scale that matters for the theoretical model is λ/n^* . Here, we used $n^* = n_0$. The theoretical model

(blue dashed line) features a kink at large values of k , which is located at $k = 4\pi n^*/\lambda$ and is due to the spectral filtering. The theoretical result is simulated using a two-dimensional grid of $2^{14} \times 2^{14}$ points and averaged over 100 realizations. We find, that there is good agreement with the actual numerical data acquired through propagation, including the pronounced kink due to evanescent waves. After the kink, the theoretical spectrum features the expected ultraviolet k^{-3} behavior.

We now re-inspect the case of $\sigma = 5\lambda$, increase κ to $\kappa = 0.1\sigma^{3/2}$ and aim at obtaining a qualitative understanding of the dynamics of the evolution of the spectra. This is shown in Fig. 4(b). The initial and final dashed curves correspond to the models (dashed curves) shown in Fig. 4(a). At an early stage ($z = 62\lambda$), where only a few vortices nucleated, the numerical spectrum (red solid line) resembles the spectrum of the the paraxial prediction (red dashed line). Upon further propagation, the peak is blue-shifted, i.e. to larger values of k . Ultimately, at $z = 1266\lambda$, the spectrum features the characteristic distribution of the evanescently filtered random spectrum - shown as the blue dashed line in (b), which is equivalent to (a) as we chose $n^* = n_0$.

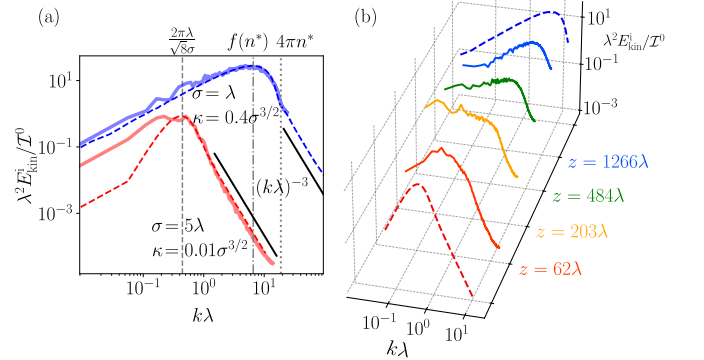


FIG. 4. (a) The incompressible kinetic energy as function of the wave vector k for a paraxial case (red) and a vectorial, nonparaxial case (blue). The dashed lines correspond to the theoretical models and the solid lines to the numerics. The black solid lines show the k^{-3} ultraviolet asymptotics. (b) The dashed lines correspond to the theoretical calculations in (a), the solid lines show the spectra upon propagation, showcasing how an initial plane wave moves from one limiting paraxial case to the random field.

In summary, we presented a statistical study of the kinetic energy of the transverse flux of light propagating in random media at the paraxial-nonparaxial interface. The expressions for the paraxial case are valid for weakly modulated refractive index media, such as beam propagation in turbulent air flow in atmospheric physics [32] or in Schlieren imaging [42]. Upon exploring the nucleation dynamics of vortices, we identified the following universal features: First, after an initial period where barely any vortices nucleate, there is a point at which, for sufficiently small correlation length, we find a scaling of vortex den-

sity of roughly $\rho_v \lambda^2 \sim (z/\lambda)^{1/3}$. Secondly, there is a kink in the nucleation rate when the correlation length is sufficiently large, similar to what has already been classically observed [41]. Third, we found that ultimately the nucleation and reconnection rates of vortices become equal and that no further complexity can be added to the field due to evanescence. Furthermore, we examined the distribution of optical incompressible kinetic energy as a function of the wave vector with attention to the paraxial - nonparaxial transition. We found that upon continuously injecting energy at the inverse correlation length, first leads to a spectrum that has the peak at that same inverse length, but upon further propagation blue-shifts and acquires a evanescently filtered random spectrum. Thus, we gain an understanding of the emergence of the driven steady state presented in Fig. 3 and the internal distribution of length scales that contribute to the kinetic energy. The dynamics is different from what is seen in fluid dynamics and quantum fluids, where energy cascades emerge upon injecting energy and dissipate at specific scales until a steady state with its characteristic slope is developed due to nonlinearity. In this paper only one length scale is fixed, i.e. the correlation length to reduce the parameter space. Therefore, this represents an effective model. Generalizing our findings to include multiple length scales, present when considering scatterers with given mean distance and dimensions, appears to be a further natural next step. Adding nonlinearity, e.g. [43] for establishing a cascade is also interesting to examine in future. Finally, an experimental realisation of the presented phenomenologies is tempting.

We would like to thank the Department of Precision and Microsystems Engineering for financial support.

* f.maucher@tudelft.nl

- [1] C. F. Bohren and D. R. Huffman, *Absorption and Scattering of Light by Small Particles* (Wiley, 1998).
- [2] K. Vynck, R. Pierrat, R. Carminati, L. S. Froufe-Pérez, F. Scheffold, R. Sapienza, S. Vignolini, and J. J. Sáenz, Light in correlated disordered media, *Reviews of Modern Physics* **95**, 045003 (2023).
- [3] A. Ishimaru, *Wave propagation and scattering in random media* (Elsevier, 1978).
- [4] M. C. W. van Rossum and T. M. Nieuwenhuizen, Multiple scattering of classical waves: microscopy, mesoscopy, and diffusion, *Rev. Mod. Phys.* **71**, 313 (1999).
- [5] R. Carminati and J. C. Schotland, *Principles of Scattering and Transport of Light* (Cambridge University Press, 2021).
- [6] L. C. Andrews, R. L. Phillips, C. Y. Hopen, and M. Al-Habash, Theory of optical scintillation, *Journal of the Optical Society of America A* **16**, 1417 (1999).
- [7] A. Patsyk, U. Sivan, M. Segev, and M. A. Bandres, Observation of branched flow of light, *Nature* **583**, 60 (2020).
- [8] S.-S. Chang, K.-H. Wu, S.-J. Liu, Z.-K. Lin, J.-B. Wu, S.-J. Ge, L.-J. Chen, P. Chen, W. Hu, Y. Xu, H. Chen, D. He, D.-Q. Yang, J.-H. Jiang, Y.-Q. Lu, and J.-H. Chen, Electrical tuning of branched flow of light, *Nature Communications* **15**, 197 (2024).
- [9] P. W. Anderson, Absence of diffusion in certain random lattices, *Phys. Rev.* **109**, 1492 (1958).
- [10] D. S. Wiersma, P. Bartolini, A. Lagendijk, and R. Righini, Localization of light in a disordered medium, *Nature* **390**, 671 (1997).
- [11] T. Schwartz, G. Bartal, S. Fishman, and M. Segev, Transport and anderson localization in disordered two-dimensional photonic lattices, *Nature* **446**, 52–55 (2007).
- [12] A. Lagendijk, B. v. Tiggelen, and D. S. Wiersma, Fifty years of anderson localization, *Physics Today* **62**, 24 (2009).
- [13] O. Dorokhov, On the coexistence of localized and extended electronic states in the metallic phase, *Solid State Communications* **51**, 381 (1984).
- [14] I. M. Vellekoop and A. Mosk, Focusing coherent light through opaque strongly scattering media, *Optics letters* **32**, 2309 (2007).
- [15] J. Bertolotti, E. G. van Putten, C. Blum, A. Lagendijk, W. L. Vos, and A. P. Mosk, Non-invasive imaging through opaque scattering layers, *Nature* **491**, 232 (2012).
- [16] H. Cao, Perspective on speckle spectrometers, *Journal of Optics* **19**, 060402 (2017).
- [17] B. Redding, S. F. Liew, R. Sarma, and H. Cao, Compact spectrometer based on a disordered photonic chip, *Nature Photonics* **7**, 746 (2013).
- [18] J. F. Nye and M. V. Berry, *Proceedings of the Royal Society of London. A. Mathematical and Physical Sciences* **336**, 165–190 (1974).
- [19] M. R. Dennis, K. O’Holleran, and M. J. Padgett, Chapter 5 singular optics: Optical vortices and polarization singularities (Elsevier, 2009) pp. 293–363.
- [20] J. Wang, J.-Y. Yang, I. M. Fazal, N. Ahmed, Y. Yan, H. Huang, Y. Ren, Y. Yue, S. Dolinar, M. Tur, and A. E. Willner, Terabit free-space data transmission employing orbital angular momentum multiplexing, *Nature Photonics* **6**, 488 (2012).
- [21] D. G. Grier, A revolution in optical manipulation, *Nature* **424**, 810–816 (2003).
- [22] A. Mair, A. Vaziri, G. Weihs, and A. Zeilinger, Entanglement of the orbital angular momentum states of photons, *Nature* **412**, 313–316 (2001).
- [23] C. F. Barenghi, R. J. Donnelly, and W. F. Vinen, *Quantized Vortex Dynamics and Superfluid Turbulence* (Springer Berlin Heidelberg, 2001).
- [24] M. R. Matthews, B. P. Anderson, P. C. Haljan, D. S. Hall, C. E. Wieman, and E. A. Cornell, Vortices in a Bose-Einstein condensate, *Phys. Rev. Lett.* **83**, 2498 (1999).
- [25] E. A. L. Henn, J. A. Seman, G. Roati, K. M. F. Magalhães, and V. S. Bagnato, Emergence of turbulence in an oscillating Bose-Einstein condensate, *Phys. Rev. Lett.* **103**, 045301 (2009).
- [26] M. V. Berry, Disruption of wavefronts: statistics of dislocations in incoherent Gaussian random waves, *Journal of Physics A: Mathematical and General* **11**, 27 (1978).
- [27] I. Freund, Optical vortices in Gaussian random wave fields: statistical probability densities, *J. Opt. Soc. Am. A* **11**, 1644 (1994).
- [28] M. V. Berry and M. R. Dennis, Phase singularities in isotropic random waves, *Proceedings: Mathematical, Physical and Engineering Sciences* **456**, 2059 (2000).
- [29] K. O’Holleran, M. R. Dennis, F. Flossmann, and M. J.

- Padgett, Fractality of light's darkness, *Phys. Rev. Lett.* **100**, 053902 (2008).
- [30] K. Staliunas, A. Berzanskis, and V. Jarutis, Vortex statistics in optical speckle fields, *Optics Communications* **120**, 23 (1995).
- [31] A. S. Bradley and B. P. Anderson, Energy spectra of vortex distributions in two-dimensional quantum turbulence, *Physical Review X* **2**, 041001 (2012).
- [32] R. Fante, Electromagnetic beam propagation in turbulent media, *Proceedings of the IEEE* **63**, 1669 (1975).
- [33] G. Osnabrugge, S. Leedumrongwatthanakun, and I. M. Vellekoop, A convergent Born series for solving the inhomogeneous Helmholtz equation in arbitrarily large media, *Journal of Computational Physics* **322**, 113 (2016).
- [34] G. Osnabrugge, M. Benedictus, and I. M. Vellekoop, Ultra-thin boundary layer for high-accuracy simulations of light propagation, *Optics Express* **29**, 1649 (2021).
- [35] E. A. Novikov, Functionals and the random-force method in turbulence theory, *Sov. Phys. JETP* **20**, 1290 (1965).
- [36] K. Furutsu, On the statistical theory of electromagnetic waves in a fluctuating medium, *J. Res. Nat. Bur. Standards D* **67**, 303 (1963).
- [37] F. Maucher, W. Krolikowski, and S. Skupin, Stability of solitary waves in random nonlocal nonlinear media, *Phys. Rev. A* **85**, 063803 (2012).
- [38] See Supplemental Material at [URL will be inserted by publisher] for the derivation of the slope of kinetic energy, which includes Ref. [35–37], and values of β for varying κ .
- [39] E. Ising, Beitrag zur Theorie des Ferromagnetismus, *Zeitschrift für Physik* **31**, 253–258 (1925).
- [40] L. P. Kadanoff, More is the same; phase transitions and mean field theories, *Journal of Statistical Physics* **137**, 777–797 (2009).
- [41] J. J. Metzger, R. Fleischmann, and T. Geisel, Universal statistics of branched flows, *Phys. Rev. Lett.* **105**, 020601 (2010).
- [42] G. S. Settles, *Schlieren and Shadowgraph Techniques* (Springer Berlin Heidelberg, 2001).
- [43] A. Nardi, A. Morandi, R. Pierrat, A. Goetschy, X. Li, F. Scheffold, and R. Grange, Mesoscopic light transport in nonlinear disordered media, *Phys. Rev. Res.* **7**, 023323 (2025).
-

Supplemental Materials: The Dynamics of the Transverse Optical Flux in Random Media

DERIVATION OF EQ.(4) IN THE MAIN TEXT

Gauss's law of Maxwell's equations without sources is given by $\nabla \cdot (\epsilon \mathbf{E}) = 0$. We see that if the permittivity ϵ varies spatially slowly on the scale of the wavelength, i.e. $|\nabla \epsilon / \epsilon| \ll k_0$, then we can approximate $\nabla \cdot \mathbf{E} \approx 0$. This reduces the wave equation Eq. (1) to the vector Helmholtz equation. In case of the incident x -polarized wave, its propagation is given by

$$\nabla^2 E_x(\mathbf{r}) + k(\mathbf{r})^2 E_x(\mathbf{r}) = 0. \quad (\text{S1})$$

Assuming that a slowly varying envelope U of $E_x = U e^{ik_0 z}$ with $k_0 = \frac{2\pi}{\lambda} n_0$ satisfies $|\partial_{zz} U| \ll |k_0 \partial_z U|$, we can perform the slowly-varying envelope approximation. Linearisation in η yields the paraxial wave equation for U :

$$2ik_0 \partial_z U = -\nabla_{\perp}^2 U - \frac{4\pi}{\lambda} \eta k_0 U. \quad (\text{S2})$$

We define the kinetic energy E_{kin} at each z -plane as

$$E_{\text{kin}}(z) = \int |\nabla_{\perp} U(\mathbf{r}_{\perp}, z)|^2 d^2 r_{\perp}, \quad (\text{S3})$$

such that E_{kin} satisfies $\frac{\delta E_{\text{kin}}}{\delta U^*} = 2ik_0 \partial_z U$ when $\eta \equiv 0$. Here, U^* denotes the complex conjugate of U . The spatial derivative of the averaged kinetic energy along the direction of wave propagation is:

$$\partial_z \langle E_{\text{kin}} \rangle = i \frac{2\pi}{\lambda} \left\langle \int \eta (U^* \nabla_{\perp}^2 U - U \nabla_{\perp}^2 U^*) d^2 r_{\perp} \right\rangle. \quad (\text{S4})$$

Since the rapid oscillating term $e^{ik_0 z}$ is factored out, U varies on a much longer length scale in the z -direction than in the x and y -directions. As a result, the ratio between correlation length σ of the fluctuation of refractive index and the variation length scale in z -direction is much smaller than the ratio in the (x, y) -plane. Therefore, it might appear reasonable to apply Markov approximation, i.e. assume that the refractive index fluctuation is delta-correlated in z direction. With that, the correlator of η becomes

$$\langle \eta(\mathbf{r}) \eta(\mathbf{r}') \rangle = C_{\perp}(\mathbf{r}_{\perp} - \mathbf{r}'_{\perp}) \delta(z - z'), \quad (\text{S5})$$

and the corresponding transverse correlation function is

$$C_{\perp}(\mathbf{r}_{\perp}) = \frac{\kappa^2}{2\pi\sigma^2} e^{-\frac{r_{\perp}^2}{2\sigma^2}}. \quad (\text{S6})$$

By applying the Furutsu-Donsker-Novikov formula [35, 36]

$$\langle \eta U \rangle = \int_{-\infty}^z \int \left\langle \frac{\delta U(\mathbf{r}_{\perp}, z)}{\delta \eta(\mathbf{r}'_{\perp}, z')} \right\rangle \langle \eta(\mathbf{r}_{\perp}, z) \eta(\mathbf{r}'_{\perp}, z') \rangle d^2 r'_{\perp} dz' \quad (\text{S7})$$

to Eq. (S4), and following similar derivation steps in Ref. [37], we obtain

$$\begin{aligned} \partial_z \langle E_{\text{kin}} \rangle &= -\frac{4\pi^2}{\lambda^2} \nabla_{\perp}^2 C_{\perp}(\mathbf{r}_{\perp}) \Big|_{\mathbf{r}_{\perp}=0} \left\langle \int |U|^2 d^2 r_{\perp} \right\rangle \\ &= -\frac{4\sqrt{2}\pi^{5/2}\sigma}{\lambda^2} \nabla_{\perp}^2 C(\mathbf{r}_{\perp}, 0) \Big|_{\mathbf{r}_{\perp}=0} \left\langle \int |E_x|^2 d^2 r_{\perp} \right\rangle \\ &= \frac{4\pi\kappa^2}{\sigma^4\lambda^2} \mathcal{I}_x. \end{aligned} \quad (\text{S8})$$

The evolution of the ensemble averaged kinetic energy is a linear function of the propagation distance z . If we do not ensemble average, there is a Brownian motion around that linear trend.

VALUES OF β FOR VARYING κ

To provide further context to the approximate value of $\beta = 1/3$ we show the evolution of the vortex density $\rho_v \lambda^2$ upon propagation and fits from which we extract the value of β . This is shown in Fig. S1.

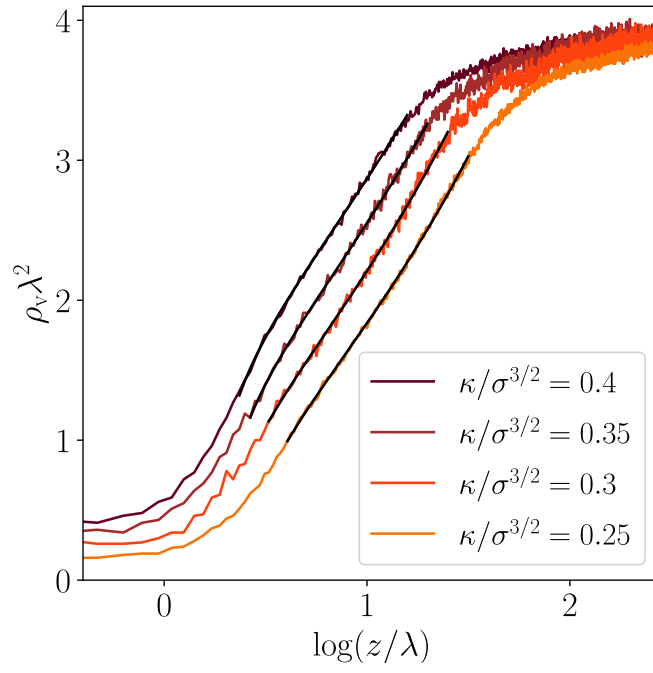


FIG. S1. Evolution of vortex number per unit area ρ_v for $\sigma = 0.5\lambda$ and $\kappa/\sigma^{3/2} = 0.25, 0.3, 0.35, 0.4$. The black solid lines show the fit as described in the main text yielding $\beta = 0.36, 0.34, 0.30, 0.27$.